

Cite this: *Sustainable Energy Fuels*,  
2021, 5, 5717

# Novel single pass biogas-to-diesel process using a Fischer–Tropsch catalyst designed for high conversion†

Chelsea L. Tucker,  ‡\*<sup>a</sup> Ankur Bordoloi <sup>b</sup> and Eric van Steen <sup>a</sup>

The decentralized production of low carbon fuels using the Fischer–Tropsch synthesis requires a less complex and more cost-effective process design. This can be achieved by operating the Fischer–Tropsch process in single pass mode (*i.e.*, without recycle), which allows for omission of the air separation unit, CO<sub>2</sub> removal step and the energy-intensive recompression. However, single pass mode necessitates operating the Fischer–Tropsch synthesis at a higher CO conversion than typically seen in industry (resulting in high H<sub>2</sub>O and low CO and H<sub>2</sub> partial pressures). These harsh conditions cause a significant decrease in the C<sub>5+</sub> yield as a consequence of the increase in the selectivity for the formation of CH<sub>4</sub> and CO<sub>2</sub>. Modification of an industrial Pt–Co/Al<sub>2</sub>O<sub>3</sub> catalyst with manganese resulted in increased fuel production of up to 14 C-% under high conversion conditions. Here, we present a technical analysis of a novel single pass biogas-to-diesel process that can operate off-grid in remote regions, focusing on counteracting the loss of yield under single pass operation by adjusting the Fischer–Tropsch conversion ( $X_{\text{CO}} = 60\text{--}90\%$ ), catalyst characteristics (Pt–Co/Al<sub>2</sub>O<sub>3</sub> vs. Mn–Pt–Co/Al<sub>2</sub>O<sub>3</sub>) and refining configuration (with and without a hydrocracker). The optimal case,  $X_{\text{CO}} = 80\%$  using a Mn–Co/Al<sub>2</sub>O<sub>3</sub> catalyst results in a production rate of 246 bbl per day of on-spec distillate from 400 kmol h<sup>−1</sup> biogas together with the net power generation of 1.8 MW.

Received 24th August 2021  
Accepted 15th October 2021

DOI: 10.1039/d1se01299a

rsc.li/sustainable-energy

## Introduction

Sustainable Development Goal 7 (SDG 7) adopted by the United Nations General Assembly aims to give access to affordable, sustainable, and modern energy to all. Hence, there is growing global momentum to substantially increase the share of renewable energy in the energy mix by 2030. A significant part of the energy world-wide is used for transportation, and technologies that can produce transportation fuels from locally available, renewable carbon-based resources are vital for ensuring this goal is met.

The Fischer–Tropsch process can produce carbon-neutral fuels from localized carbonaceous material such as organic waste, biomass,<sup>1–3</sup> or biogas.<sup>4,5</sup> However, the Fischer–Tropsch process is typically implemented on a large industrial scale (using either coal or natural gas as a feedstock) due to process complexity and high capital costs.<sup>6</sup> The application of this

process on a small, decentralized scale using biogas requires a reduction in both operational complexity and capital costs. The latter may be achieved by omitting the rather costly air separation unit from the design of the process (this unit can contribute up to 23% of the total cost),<sup>7,8</sup> and using air rather than oxygen in the reformer. Syngas generation without an air-separation unit produces a nitrogen-rich synthesis gas, thus necessitating the removal of the recycle streams in the process. Hence, the Fischer–Tropsch synthesis is required to operate in single pass mode under high CO conversions to maximize the yield of liquid hydrocarbons.

We previously reported<sup>9,10</sup> on the design of a novel single pass biogas-to-diesel process operating at high CO conversions for decentralized fuel production (see Fig. 1), called *Decentralized Diesel*. The single pass design negates the need for energy-intensive CO<sub>2</sub> removal (as dilute synthesis gas can be used), as well as recompression within the recycle streams. Non-recycled gas is used to generate power, enabling off-grid applications.

Other single pass Fischer–Tropsch systems have been previously investigated<sup>11–14</sup> with promising results, albeit without a consideration of using higher CO conversions as a mechanism for enhancing fuel yields. The fundamental problem associated with operating the Fischer–Tropsch synthesis at a high CO conversion is the reduced activity and selectivity<sup>15–17</sup> (due to high partial pressures of H<sub>2</sub>O and low partial pressures of CO and H<sub>2</sub> within the reactor). For a slurry

<sup>a</sup>Catalysis Institute, Department of Chemical Engineering, University of Cape Town, Rondebosch, Cape Town, South Africa. E-mail: c.l.tucker@rug.nl

<sup>b</sup>CSIR Indian Institute of Petroleum, Dehradun, India

† Electronic supplementary information (ESI) available. See DOI: 10.1039/d1se01299a

‡ Current address: Green Chemical Reaction Engineering, Engineering and Technology Institute Groningen, University of Groningen, Nijenborgh 4, 9747 AG Groningen, The Netherlands.



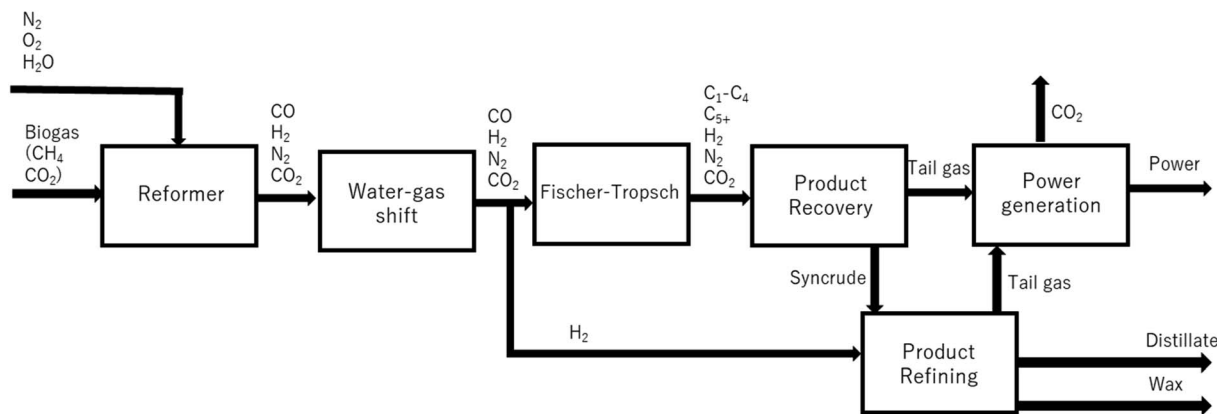


Fig. 1 Schematic of the small-scale, single pass biogas-to-distillate process.

bed reactor system, the selectivity for the formation of the undesired products,  $\text{CH}_4$  and  $\text{CO}_2$ , increases significantly above CO conversion levels of 70% for a standard industrial cobalt-based Fischer-Tropsch catalyst<sup>15,17,18</sup> resulting in a strong decrease in the  $\text{C}_{5+}$  yield, thus rendering operation at CO conversions above this limit practically unfeasible.

This issue can be negated by a Fischer-Tropsch catalyst specifically designed for high conversions operation. We recently developed a manganese-promoted cobalt catalyst that yields far better productivity at high CO conversions than the standard industrial cobalt catalyst. The manganese-promoted catalyst,  $\text{Mn-Pt-Co/Al}_2\text{O}_3$  (ref. 9 and 19) with a Mn : Co molar ratio of 0.15 decreased the selectivity towards  $\text{CH}_4$  (by 12 C-%) and  $\text{CO}_2$  (by 7 C-%) at high CO conversion ( $X_{\text{CO}} = 90\%$ ) when compared to standard industrial  $\text{Pt-Co/Al}_2\text{O}_3$ . This led to a significant enhancement of fuel yield ( $\text{C}_{5+}$ ) up to 14 C-% at  $X_{\text{CO}} = 90\%$  (see Fig. 2).

The aim of this investigation is to determine the optimal Fischer-Tropsch conversion and refining configuration for a single pass biogas-to-diesel process using (i) a standard industrial catalyst  $\text{Pt-Co/Al}_2\text{O}_3$ , and (ii) a catalyst designed for high conversion environments  $\text{Mn-Pt-Co/Al}_2\text{O}_3$ .

The design of a once-through biogas-to-distillate process will be evaluated using an Aspen Plus® model. A total of 16 cases

will be tested including: four different levels of conversion in the Fischer-Tropsch synthesis (60%, 70%, 80% and 90%), using two different cobalt-based Fischer-Tropsch catalysts ( $\text{Pt-Co/Al}_2\text{O}_3$  and  $\text{Mn-Pt-Co/Al}_2\text{O}_3$ ) and a partial refining plant with and without hydrocracking.

For the purposes of representing the design *via* carbon and energy balances, a base case will be used: a once-through system operating with a standard industrial  $\text{Pt-Co/Al}_2\text{O}_3$  catalyst in the Fischer-Tropsch synthesis (operated at  $X_{\text{CO}} = 60\%$ ) and a partial refining section that includes a hydrocracker.

## Model development

The following assumptions were made in the development of the once-through biogas-to-distillate Aspen Plus® model.

### Overall design

The once-through biogas-to-distillate plant, the development of which is described elsewhere,<sup>9</sup> is shown in Fig. 1. In this design, (sweet) clean biogas is reformed to synthesis gas and the ratio of  $\text{H}_2$  : CO is adjusted in a water-gas shift unit. Some of the hydrogen is separated from the stream using a hydrogen separation membrane.<sup>20</sup> The syngas is subsequently converted in the Fischer-Tropsch reactor; the products of the Fischer-Tropsch synthesis are separated into light gases, hydrocarbons in the diesel range and wax. The light gases (tail gas) are used to co-generate power *via* a gas fed power plant. Wax is hydrocracked<sup>21</sup> to improve diesel yield. The process was modelled

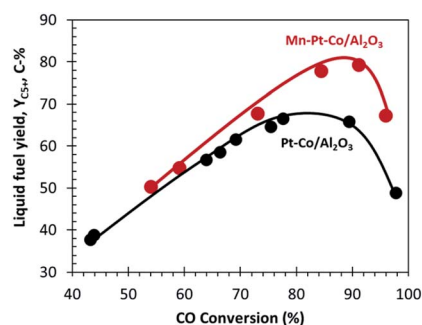


Fig. 2 The yield of  $\text{C}_{5+}$  as a function of CO conversion for standard industrial  $\text{Pt-Co/Al}_2\text{O}_3$  and industrial  $\text{Mn-Pt-Co/Al}_2\text{O}_3$  Mn : Co = 0.15 mol/mol.<sup>9,19</sup>

Table 1 Inputs to model of components based on the anaerobic digestion of 400 tons municipal solid waste (MSW) per day

Component	Molar flow (kmol h <sup>-1</sup> )
Methane ( $\text{CH}_4$ )	300
Carbon dioxide ( $\text{CO}_2$ )	100
Oxygen ( $\text{O}_2$ )	0–250
Water ( $\text{H}_2\text{O}$ )	0–400
Nitrogen ( $\text{N}_2$ )	0–940



using three Aspen Plus® simulations: syngas cleaning and compression, separation and refining and power production. The hydrogen separation membrane,<sup>20</sup> Fischer–Tropsch reaction<sup>15</sup> and hydrocracker<sup>21</sup> were modelled on Excel using empirical data.

The feed to the plant consists of 400 kmol h<sup>-1</sup> clean biogas (molar feed rates into the process are given in Table 1). This is equivalent to biogas produced from 400 t per day of organic municipal solid waste which is roughly equal to the amount of organic waste produced in Sub-Saharan cities with populations between 200 000 (ref. 22) and 900 000 (ref. 23) (region and income level dependent). These populations are equivalent to well-known cities such as Gaborone, Botswana (232 000) and Kigali, Rwanda (860 000), respectively.

The generation of sweet biogas (post-desulphurization), *i.e.* anaerobic digestion and gas cleanup, were not modelled (the output from these processes using various feedstocks are well documented<sup>24–26</sup>). The biogas composition (75% CH<sub>4</sub> and 25% CO<sub>2</sub>) was based on a methane-rich stream from the anaerobic digestion of organic waste.<sup>24</sup>

Air and water are being fed to the reformer. The chosen ranges for oxygen and water vapor flow rate were based on similar studies used for autothermal reforming, steam reforming and tri-reforming.<sup>27–29</sup> The nitrogen flow rate was calculated according to the oxygen flow rate and the standard composition of air.

### Syngas generation and compression

The syngas generation and compression section comprise a tri-reformer, water gas shift reactor, compression system and hydrogen separation (split ratio defined by requirements in the hydrocracker). Fig. 3 shows the Aspen Plus® simulation of the section. The stream table belonging to the base case (*i.e.*, the Fischer–Tropsch section operating at a conversion of 60% with a Pt–Co/Al<sub>2</sub>O<sub>3</sub> catalyst and a partial refining section including a hydrocracker) can be found in ESI.†

Air and biogas are compressed to 2.7 bar (determined as optimal for maximizing CH<sub>4</sub> conversion, whilst minimizing compression requirements) and combined with water pumped to the same conditions. The air, water and biogas feed are preheated to 220 °C before being fed into the tri-reformer. The tri-reformer was modelled as an RIGIBS reactor, presuming that the exit composition is mainly controlled by chemical

equilibrium at the given outlet temperature.<sup>26,30</sup> Whilst in practice equilibrium may not be achieved, modern reforming catalysts<sup>31–34</sup> are reported to operate relatively close to equilibrium exit concentrations,<sup>26,35,36</sup> especially at high temperatures.<sup>35</sup> Thermodynamic models driven by equilibrium have been shown to satisfactorily estimate the O<sub>2</sub> consumption<sup>31</sup> and H<sub>2</sub>/CO ratios at temperatures above 750 °C (ref. 37) in reformers. It must be noted that CH<sub>4</sub> conversions and CO<sub>2</sub> conversions may deviate slightly from equilibrium at temperatures lower than 750 °C due to inaccuracies in the modelling of coke formation.<sup>31</sup>

The tri-reformer was designed to deliver a H<sub>2</sub>/CO ratio sufficient for the Fischer–Tropsch reactor, whilst the water–gas shift unit was designed to provide excess hydrogen needed for the hydrocracker (as determined by the H<sub>2</sub> : HC ratio requirements). The WGS conversion and exit H<sub>2</sub>/CO ratio were determined by excess steam addition and inlet temperature (determined by the exit temperature of the feed cooler). The water–gas reactor was modelled as an adiabatic plug flow reactor using an empirical power law (eqn (1)) with parameters for the noble metal catalyst, 0.5%Pt/TiO<sub>2</sub>.<sup>38</sup> The catalyst, 0.5% Pt/TiO<sub>2</sub>, was used due to its relatively high water–gas shift activity at low-to-medium temperatures, which facilitates single stage operation rather than the more classical two-stage water–gas shift process.<sup>39</sup>

$$r = k_0 \times e_a^{-\frac{E}{RT}} \times \frac{p_{\text{CO}}^{0.5} \times p_{\text{H}_2\text{O}}}{p_{\text{H}_2}^{0.7}} \times (1 - \beta) \quad (1)$$

with,  $r$ : rate of CO-consumption (mol s<sup>-1</sup> g<sub>cat</sub><sup>-1</sup>),  $k_0$ : Arrhenius parameter (0.31 mol s<sup>-1</sup> g<sub>cat</sub><sup>-1</sup>),  $E$ : activation energy (10.8 kcal mol<sup>-1</sup>),  $\beta = \frac{p_{\text{CO}_2} \times p_{\text{H}_2}}{K_{\text{Eq}} \times p_{\text{CO}} \times p_{\text{H}_2\text{O}}}$ , approach of the product composition to equilibrium<sup>38</sup>

The water–gas shift reactor product stream is cooled to 35 °C and water is knocked out before entering the 2-stage compressor system (compression ratio = 2.7) with inter-stage cooling. Water is knocked out at each stage.

After the final compressor, a stream of hydrogen is separated off from the Fischer–Tropsch feed stream to be used in the hydrocracker. To achieve this, a hydrogen selective polymeric membrane (Polyimide Matrimid®), which has a good trade-off between the permeability and H<sub>2</sub>/CO<sub>2</sub> and H<sub>2</sub>/N<sub>2</sub> selectivity.<sup>20</sup> Permeability and selectivity values for the syngas components

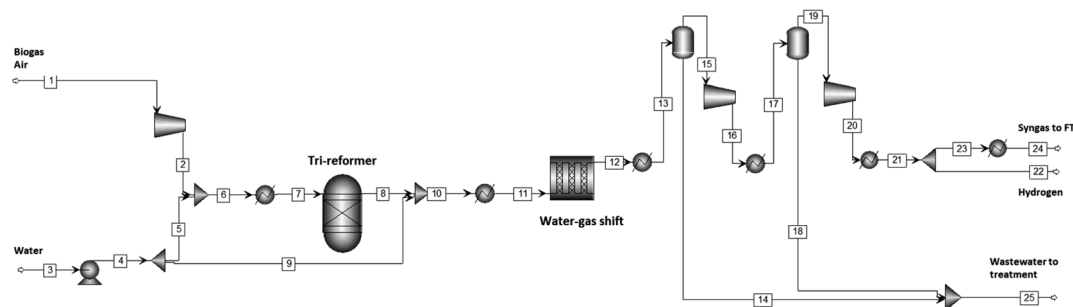


Fig. 3 Aspen model for syngas generation and compression with a clean biogas feed.



Table 2 Polymeric hydrogen separation membrane including the permeabilities and selectivity's toward components of syngas<sup>20</sup>

Membrane type	Permeability, barrer <sup>a</sup>				Ideal selectivity				Exp. conditions	
	H <sub>2</sub>	CO <sub>2</sub>	N <sub>2</sub>	CO	CH <sub>4</sub>	H <sub>2</sub> /N <sub>2</sub>	H <sub>2</sub> /CO <sub>2</sub>	H <sub>2</sub> /CO	T °C	Ref.
Polyimide Matrimid®	23.9	6.1	0.19	0.44	—	133.9	4.0	54.8	30	20

<sup>a</sup> 1 barrer = 10<sup>-10</sup> cm<sup>3</sup> (STP) cm (cm<sup>2</sup> per s per cmHg).

through Matrimid® have been well established (see Table 2).<sup>20,40–42</sup> The flux of various species through the membrane was calculated using:

$$N_i = \frac{P_{M_i}}{l_M} (\Delta P)$$

where  $N_i$  is the molar *trans*-membrane flux of species  $i$  (cm<sup>3</sup> (STP) per (cm<sup>2</sup> per s)),  $P_{M_i}$  is the permeability of species  $i$  (cm<sup>3</sup> (STP)cm per (cm<sup>2</sup> per s per cm Hg)),  $l_M$  is the membrane thickness (cm) and  $\Delta P$  is the pressure difference across the membrane (cm Hg).

Both raffinate and permeate concentrations were calculated based on these permeabilities as reported by David *et al.*<sup>20</sup> The flux through the Matrimid® membrane can be controlled by permeate pressure and membrane area.<sup>43</sup> In this case, the lower boundary for permeate pressure was set at *ca.* 8.8 bar, to make sure that the hydrogen can be recompressed for the hydrocracker in 1 stage with a compression ratio less than 4.

### Fischer–Tropsch reactor

The Fischer–Tropsch reactor was modelled using empirical selectivity data taken from our previous studies Pt–Co/Al<sub>2</sub>O<sub>3</sub> and Mn–Pt–Co/Al<sub>2</sub>O<sub>3</sub>, molar Mn : Co = 0.15 (ref. 15 and 19) and rate data based on.<sup>44</sup>

Experimental data of selectivity (CH<sub>4</sub>, CO<sub>2</sub>, C<sub>5+</sub>) and chain growth probability as a function of conversion obtained with these two catalysts were used for this purpose (see Fig. 4) and they were fitted to exponential functions of the form ( $a \times eb^{X_{CO}} + c$ ) for computational simplicity, with constants determined using least squares regression. The chain growth probability decreases significantly with increased CO conversion. This is due to enhanced water–gas shift activity at high H<sub>2</sub>O partial pressures, which results in an increase in H<sub>2</sub>/CO ratios, and an inhibition of chain growth.<sup>15</sup> For instance, at CO conversions of  $X_{CO} = 60\%$ ,  $70\%$ ,  $80\%$  and  $90\%$  the alpha values are 0.91, 0.90, 0.88 and 0.83 respectively for Pt–Co/Al<sub>2</sub>O<sub>3</sub>. The fitting of this data can be seen in Fig. 4 and the constants for the various fits are presented in ESI.† The product selectivity for the relative formation of long chain hydrocarbons (in the range C<sub>5</sub>–C<sub>80</sub>) was determined using a standard, single alpha ASF distribution, from which the product distribution at selected conversions were obtained.

The olefin content in the range C<sub>2</sub>–C<sub>11</sub> is not only significant (between 65% and 10%)<sup>15,46</sup> but also strongly dependent on conversion. The olefin/paraffin ratio for each catalyst was determined as a function of carbon number experimentally. The olefin content in the fraction of hydrocarbons was fitted using an empirical model as a function of conversion and

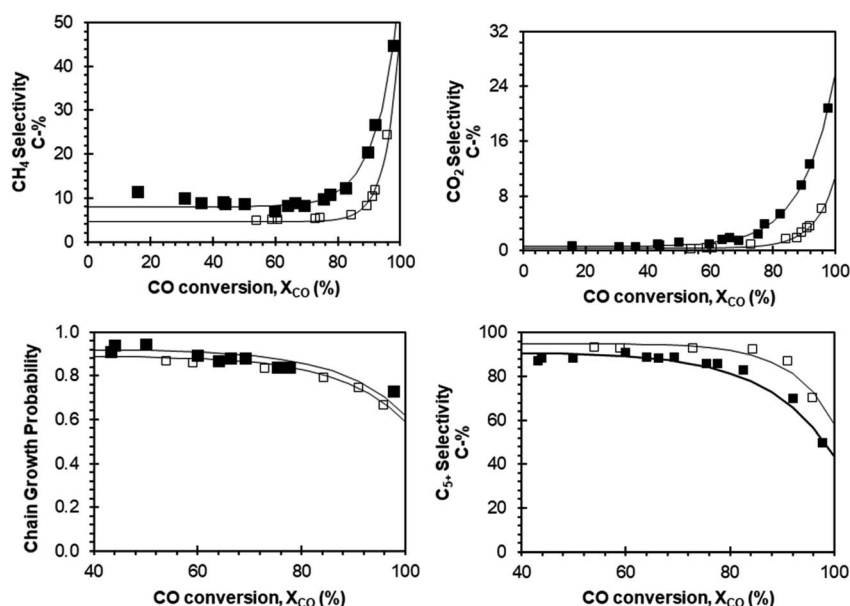


Fig. 4 Empirical modelling of the Fischer–Tropsch products as a function of conversion based on selectivity data from our previous study<sup>19,45</sup> for Pt–Co/Al<sub>2</sub>O<sub>3</sub> (closed symbols) and Mn–Pt–Co/Al<sub>2</sub>O<sub>3</sub> with a molar ratio of Mn : Co = 0.15 mol/mol (open symbols).



carbon number. The olefin content in the fraction of hydrocarbons  $C_{11}$ – $C_{22}$  is *ca.* 5%.<sup>46</sup> Thus, this was used as a constant value for the olefin content in this range. The olefin content in the fraction of linear hydrocarbons  $C_{22+}$  over cobalt-based catalysts is negligible,<sup>46</sup> and hence the olefin content in this carbon number fraction was set to zero.

### Separation and refining

Wax, distillate, water (incl. aqueous products) and tail gas (a mixture of  $H_2$ ,  $CO$ ,  $CO_2$ ,  $CH_4$ ,  $N_2$  and  $C_2$ – $C_{10}$ ), are separated out in the effluent of the Fischer–Tropsch synthesis and the distillate is refined to meet diesel specifications (see Fig. 5). The stream table for the base case separation and refining section can be found in ESI.†

The first separation occurs in the Fischer–Tropsch reactor itself (modelled as a flash tank at the conditions of the Fischer–Tropsch reactor, *i.e.*, 220 °C and 20 bar). The vapor emanating from the Fischer–Tropsch reactor is fed initially into a water-knock out and then into a pressurized cold condensate flash tank where distillate is separated off from the water and tail gas. The subsequent flash tank knocks out Fischer–Tropsch product water. The pressurized tail gas is then fed to the power generation section, which consists of an energy recovery gas turbine for the pressurized stream, and a steam turbine.

### Power generation

The tail-gas from the partial refinery is fed to a power generation unit (see Fig. 6). Two tail gas streams exist, a high-pressure stream from cold condensate and water separator and a depressurized stream from the atmospheric distillation column. The pressurized tail gas is fed first through a gas turbine to generate power. The two atmospheric tail gas streams are then

combined with air at atmospheric pressure and combusted; the heat is being used to generate steam which is fed to a steam turbine, thereby generating power for the plant and excess power. The combustion was modelled using an RGIBBS model.

### Distillate specifications

The term ‘diesel’ refers to a mixture of roughly  $C_{10}$ – $C_{22}$  straight-chain hydrocarbons that meets region-legislated specifications of cetane number, flash point, distillation profile and cloud point (see ESI† for regional diesel specifications for the US, EU, Africa and South Africa). Although it would be preferable to meet the specifications for diesel, this is not feasible due to the inherent low density of Fischer–Tropsch fuels. Thus, the fuel produced in this process can be more accurately termed on spec distillate (*i.e.* meeting all specifications of diesel excluding density). To ensure these specifications were met, the following product characteristics were calculated:

- Flash point
- Cetane number
- Cloud point
- Distillation curve

Fischer–Tropsch LTFT distillate typically has a very low sulphur and aromatic content,<sup>47</sup> neither of which were modelled in this study.

Flash points were calculated using the Pensky–Martens flash point estimation (ASTM D-93)<sup>48</sup> as implemented in Aspen Plus®. The cetane number of the diesel from the atmospheric distillation column was calculated using the correlation from Ghosh and Jaffe:<sup>49</sup>

$$CN = \frac{\sum v_i \beta_i CN_i}{\sum v_i \beta_i}$$

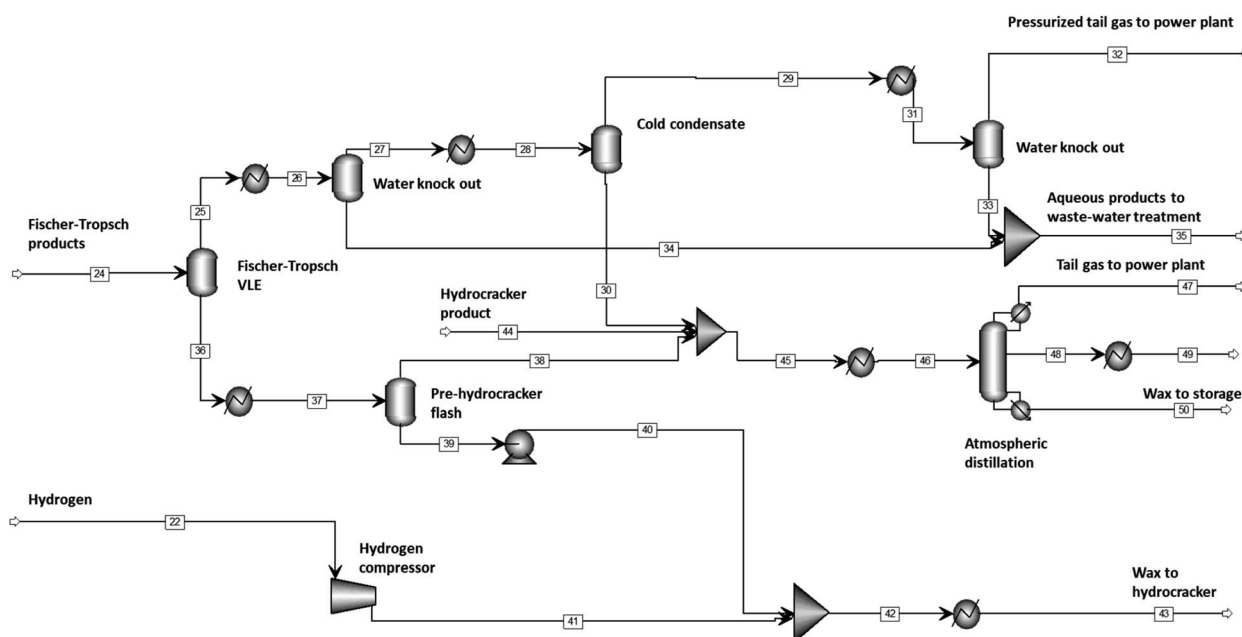


Fig. 5 Aspen model for Fischer–Tropsch product separation and distillate refining.



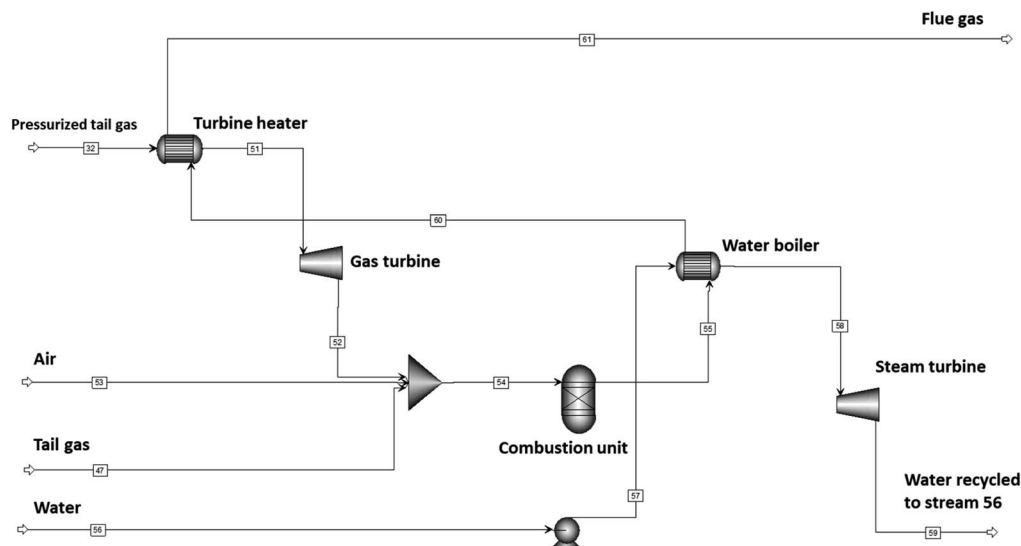


Fig. 6 Aspen model for the power plant.

where CN represents the cetane number of the mixture,  $\beta$  is a correlation factor based on a blend value that differs for  $n$ -paraffins and olefins,  $\nu_i$  is the volume fraction of compound  $i$  in the fuel, whilst  $CN_i$  is the lumped cetane number of compound  $i$ . Cloud points were calculated using the correlation:<sup>50</sup>

**Table 3** Summary of key unit operations and the Aspen Plus® block or modelling algorithm used in the development of the once-through biogas-to-distillate plant

Unit operation	Aspen Plus® block or modelling algorithm	Input conditions
Tri-reformer	RGibbs	$T = 750\text{ °C}/P = 2.7\text{ bar}$ /selectivities calculated at equilibrium
Water-gas shift reactor	RPlug	Adiabatic/ $T_0 = 280\text{ °C}/P = 2.7\text{ bar}$ /rate calculated according to ref. 38
Biogas and air compressor	Compr	$P = 2.71\text{ bar}$
Feed water pump	Pump	$P = 2.71\text{ bar}$
Compressor feed cooler	Compr	$P = 2.71/T = 35\text{ °C}$
Fischer-Tropsch feed compressor	Compr/Flash/Heater	$P_1 = 7.3\text{ bar}/P_2 = 20\text{ bar}$ /inter-stage cooling = $35\text{ °C}$ /inter-stage water knockout/isentropic efficiency = 76%
Membrane	Modelled using eqn (1) and data from ref. 20	Selectivity and permeability based on ref. 20
Fischer-Tropsch reactor	Modelled using experimental data from ref. 15	$X_{CO} = 60, 70, 80\text{ and }90\%$
Fischer-Tropsch feed heater	Heater	$P = 20\text{ bar}/T = 220\text{ °C}$
Hydrogen compressor	Compr	$P_{\text{exit}} = 35\text{ bar}$
Cold condensate	Flash	$P = 19.5\text{ bar}/T = 50\text{ °C}$
Pre-hydrocracker flash	Flash	$P = 1\text{ bar}/T = 370\text{ °C}$
Water flash	Flash	$P = 19\text{ bar}/T = 35\text{ °C}$
Hydrocracker pump	Pump	$P_{\text{exit}} = 35\text{ bar}$
Atmospheric distillation	RadFrac	$P = 1\text{ bar}/T = 150\text{--}200\text{ °C}$ /reboiler duty = 90–210 kW/partial condenser/reflux ratio = 0.2/8 stages/feed stage = 2/split stage = 7
Hydrocracker	Modelled using experimental data from ref. 21	Conversion = 81%, $P = 35\text{ bar}, T = 370\text{ °C}$
Fischer-Tropsch product cooler	Heater	$P = 19.5\text{ bar}/T = 50\text{ °C}$
Water knockout cooler	Heater	$P = 19\text{ bar}/T = 35\text{ °C}$
Hydrocracker heater	Heater	$P = 35\text{ bar}/T = 370\text{ °C}$
Distillation feed heater	Heater	$P = 1\text{ bar}/T = 150\text{--}200\text{ °C}$
Power generation		
Gas turbine	Compr (turbine)	$P_{\text{exit}} = 1\text{ bar}$ /isentropic efficiency = 38%
Steam turbine	Compr (steam)	$P_{\text{exit}} = 1\text{ bar}$ /isentropic efficiency = 76%
Combustion unit	RGibbs	Adiabatic, $P = 1\text{ bar}$
Power plant feed heater	HeatX	Counter-current, $T_{\text{cold,out}} = 390\text{ °C}, \Delta T = 10\text{ °C}$
Steam boiler	HeatX	Counter-current, $T_{\text{cold,out}} = 620\text{ °C}, \Delta T = 10\text{ °C}$
Condenser	HeatX	Counter-current, $T_{\text{cold,out}} = 50\text{ °C}, \Delta T = 10\text{ °C}$
Water pump	Pump	$P_{\text{exit}} = 100\text{ bar}$



$$CP = -267.5332SG + 0.1315T_{10\%} + 0.7837T_{50\%} - 0.4301T_{90\%} + 89.1003\%$$

where CP is the cloud point in °C, SG is the specific gravity of the distillate, and  $T_{10\%}$ ,  $T_{50\%}$  and  $T_{90\%}$  are points on the cumulative distribution distillation curve which was modelled using the atmospheric equivalent boiling points of paraffins.<sup>51</sup>

Using the biogas-to-distillate plant model and the results from an in-depth sensitivity analysis (see ESI†), an optimized system was developed using the conditions shown in Table 3.

### Carbon yield definitions

The carbon yield reported in this study are, unless otherwise specified, based on the amount of carbon contained in biogas (incl. carbon dioxide plus methane). Yields based on methane only will be stated as such. Carbon yields for this process are calculated as follows.

$$\text{Carbon yield of CO after the water-gas shift unit} = \frac{n_{\text{CO,WGS}}}{n_{\text{CH}_4,\text{feed}} + n_{\text{CO}_2,\text{feed}}}$$

$$\text{Yield of CO from methane after the water-gas shift unit} = \frac{n_{\text{CO,WGS}}}{n_{\text{CH}_4,\text{feed}}}$$

$$\text{Hydrocarbon yield} = \frac{\sum_{i=1}^{80} n_{C_i,X} \times i}{n_{\text{CH}_4,\text{feed}} + n_{\text{CO}_2,\text{feed}}}$$

$$\text{Distillate yield} = \frac{\sum_{i=10}^{22} n_{C_i,\text{distillate}} \times i}{n_{\text{CH}_4,\text{feed}} + n_{\text{CO}_2,\text{feed}}}$$

$$\text{Overall distillate yield} = \frac{\sum_{i=10}^{22} n_{C_i,\text{distillate}} \times i}{n_{\text{CH}_4,\text{feed}} + n_{\text{CO}_2,\text{feed}}}$$

$$\text{Overall distillate yield from methane} = \frac{\sum_{i=10}^{22} n_{C_i,\text{distillate}} \times i}{n_{\text{CH}_4,\text{feed}}}$$

with  $i$ : carbon number,  $n_{\text{CO}_2,\text{feed}}$ : moles of carbon dioxide in feed,  $n_{\text{CH}_4,\text{feed}}$ : moles of methane in feed,  $n_{\text{CO,WGS}}$ : moles of carbon monoxide exiting the water-gas shift reactor,  $n_{C_i,\text{FT}}$  product: moles of hydrocarbon with carbon number  $i$  in Fischer-Tropsch product, X: position in process (*i.e.*, after Fischer-Tropsch synthesis, before refining),  $n_{C_i,X}$ : moles of hydrocarbon with carbon number  $i$  at X process position,  $n_{C_i,\text{distillate}}$ : moles of hydrocarbon with carbon number  $i$  in distillate stream.

## Results and discussion

### Carbon balance (base case)

Fig. 7 shows the carbon flow diagram for the optimized base case (Pt-Co/Al<sub>2</sub>O<sub>3</sub>,  $X_{\text{CO}} = 60\%$  with hydrocracking), indicating how carbon from biogas is converted into various products across the plant. The overall feed to the plant is 400 kmol h<sup>-1</sup> methane-rich biogas, with a composition of 25% CO<sub>2</sub> and 75% CH<sub>4</sub>.

Biogas is fed into the tri-reformer operated at 750 °C and 2.7 bar (chosen based on analysis shown in ESI†), which achieves a CH<sub>4</sub> conversion of 97%. The CO<sub>2</sub> conversion is negative due to the prevalence of the water-gas shift reaction at these temperatures. The resulting syngas reacts further in the water-gas shift unit, which converts CO and H<sub>2</sub>O into CO<sub>2</sub> and H<sub>2</sub> to adjust the H<sub>2</sub> : CO ratio. After the water-gas shift reactor, the carbon yield of CO is 62 C-% (the yield of CO from methane of 83 C-%). Just before entering the Fischer-Tropsch reactor, some CO<sub>2</sub> is inadvertently removed from the stream through the H<sub>2</sub> separation membrane.

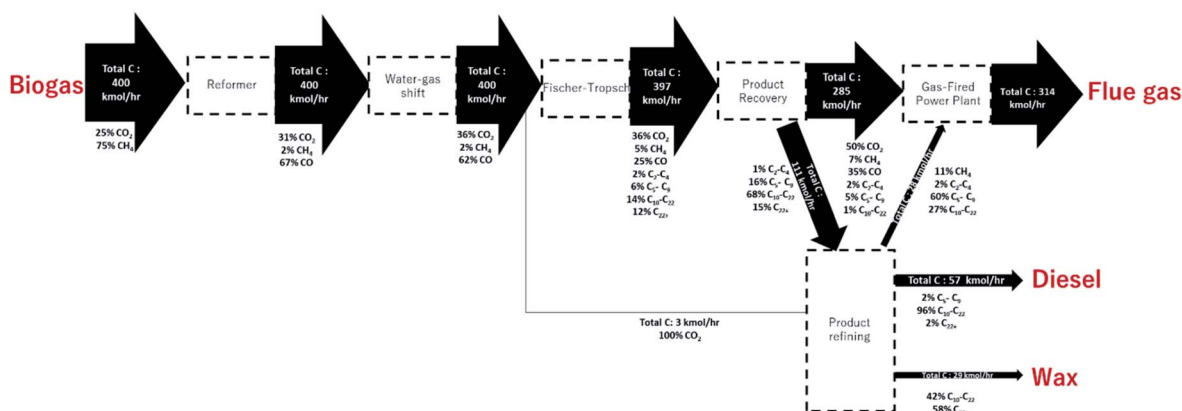


Fig. 7 Carbon flow diagram of the Fischer-Tropsch plant operating at  $X_{\text{CO}} = 60\%$  showing the distribution of carbon throughout the plant, including the distribution of carbon in (C-%) of different species in each section. Line thickness proportional to carbon flow.



The syngas stream enters the Fischer–Tropsch reactor, which converts CO (at a conversion of  $X_{\text{CO}} = 60\%$  for the base case) into longer-chain hydrocarbons. Carbon in the stream exiting the Fischer–Tropsch reactor can be found as  $\text{CO}_2$  (36 C-%), CO (25 C-%),  $\text{CH}_4$  (5 C-%),  $\text{C}_2\text{--C}_4$  (2 C-%),  $\text{C}_5\text{--C}_9$  (6 C-%),  $\text{C}_{10}\text{--C}_{22}$  (14 C-%) and  $\text{C}_{22+}$  (12 C-%). After the Fischer–Tropsch synthesis, the carbon yield to liquid hydrocarbons ( $\text{C}_{5+}$ ) is 34 C-%, with a carbon yield to distillate ( $\text{C}_{10}\text{--C}_{22}$ ) of 14 C-%. The reason for the relatively low yield of distillate is the large amount of unconverted CO and the non-selective nature of the Fischer–Tropsch synthesis itself, with a significant portion of carbon contained in wax and lower hydrocarbons. The former can be partially recovered by mild hydrocracking.

The product recovery section splits the Fischer–Tropsch products into tail gas and liquid products with flow rates of 286 kmol carbon per hour and 111 kmol carbon per hour respectively. The tail gas contains 1 C-% in the distillate range (2.8 kmol carbon per hour) whilst the liquid products contain 67 C-% in the distillate range (74.4 kmol carbon per hour). This represents a loss of 3.8% of carbon in the distillate range to the tail gas after product recovery.

The hydrocracker in this section improves the distillate yield ( $\text{C}_{10}\text{--C}_{22}$ ) from 14 C-% (after the Fischer–Tropsch synthesis) to 19 C-% (after hydrocracking, before refining). To meet the legal specifications of diesel, excluding density, the distillate is refined in an atmospheric distillation column into tail gas, distillate, and wax. This is where the largest losses of distillate ( $\text{C}_{10}\text{--C}_{22}$  hydrocarbons) occur. The wax stream has a carbon flow rate of 29 kmol carbon per hour of which 42% is in the distillate ( $\text{C}_{10}\text{--C}_{22}$ ) range. The tail gas contains 28 kmol carbon per hour, of which 27% is  $\text{C}_{10}\text{--C}_{22}$ . Entrained distillate in these two streams results in distillate losses of 12 and 8 kmol carbon per hour, respectively.

A total of 57 kmol carbon per hour on-spec distillate is produced *via* the side stream, of which 96% is  $\text{C}_{10}\text{--C}_{22}$ . The overall carbon yield of  $\text{C}_{10}\text{--C}_{22}$  in the final on-spec. distillate stream from the atmospheric distillation column is 14 C-%.

The remaining light hydrocarbons are combined with the pressurized tail gas, which contain all the remaining  $\text{CO}_2$ ,  $\text{CH}_4$  and CO. This is combusted in the power plant, resulting in a product stream of  $314 \text{ kmol h}^{-1}$  of  $\text{CO}_2$  and a gross power generation of 8.5 MW.

There is a loss of 5 C-% in the distillate yield over the refining section. These refining losses could be mitigated in a few ways. Higher yields could be obtained if the purity requirements for the distillate stream were reduced. This would result in an increase in  $\text{C}_5\text{--C}_9$  and  $\text{C}_{22}$  in the distillate stream which would shift the flash point and distillation profiles out of spec. for diesel. This would only be possible if the desired product were distillate for blending, rather than diesel. Alternatively, the wax stream could be recycled back to the hydrocracker to improve distillate yields. Whilst this would not strictly satisfy the single-pass design constraint, the wax stream is liquid and thus could be pumped without significant capital cost or energy requirements. If the entire wax stream were recycled to hydrocracker (*via* the pre-hydrocracker flash), an additional 10 kmol carbon per hour of distillate could be produced, resulting in an overall distillate yield of 17 C-%.

### Energy balance (base case)

The overall energy efficiency of the once-through reactor system and power plant was assessed by analyzing the lower heating values (LHV) of the reactants and products as well as the power production in the power plant (LHV used rather than HHV due to gaseous water product streams). Fig. 8 shows an illustration of the energy flow throughout the system for the base case of  $X_{\text{CO}} = 60\%$  with a hydrocracker.

The LHV of biogas ( $400 \text{ kmol h}^{-1}$ ) with composition 75%  $\text{CH}_4$  and 25%  $\text{CO}_2$  is *ca.* 67 MW. Throughout the *Decentralized Diesel* plant (including reformer, water–gas shift unit, Fischer–Tropsch reactor and refining section) 23 MW is lost mainly in the form of emissions and cooling water. At a moderate conversion of  $X_{\text{CO}} = 60\%$ , most of the energy leaves the system as tail gas (37 MW) to the power plant whilst only 5 MW and 2 MW are contained in the distillate and wax respectively. Considering all the product streams, the overall efficiency of the Fischer–Tropsch process (calculated by the LHV products relative to LHV of biogas) is 66%. The distillate energy efficiency is only 8% but can be further improved with appropriate heat integration. For a conversion of  $X_{\text{CO}} = 60\%$ , the gas fired power plant has an efficiency of 23%, producing only 8.5 MW (gross) from 37 MW of tail gas with a loss of 29 MW. This is significantly lower than the expected efficiency of *ca.* 30–40% for steam

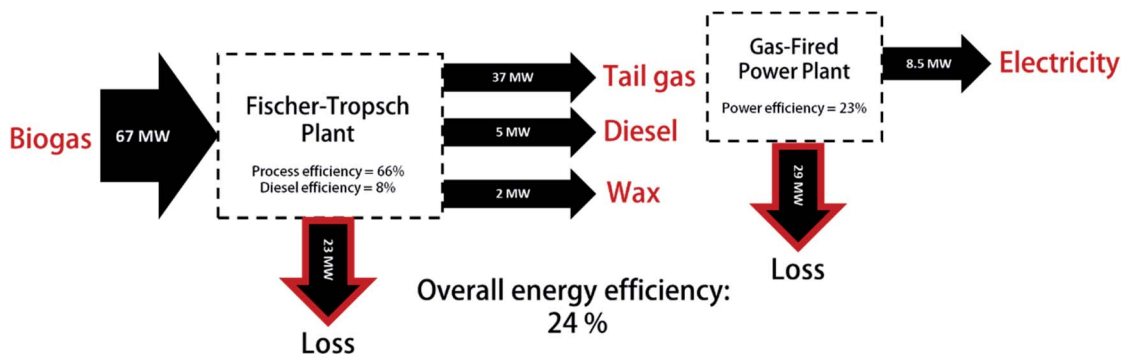


Fig. 8 Energy balance for base case design  $X_{\text{CO}} = 60\%$  for Pt–Co/ $\text{Al}_2\text{O}_3$  showing the lower heating values of reactants and products as well as the power generated from the plant.



turbines. This is due, in part, to the dilution of the feed gas with high concentrations of inert nitrogen and carbon dioxide thus reducing the maximum temperature. In addition, not all the flue gas heat could be effectively utilized in the power plant itself and may be included in plant-wide heat integration.

### Plant evaluation

The biogas-to-distillate plant was evaluated based on 16 optimized scenarios including Fischer–Tropsch conversions of  $X_{\text{CO}} = 60\%$ ,  $70\%$ ,  $80\%$  and  $90\%$ , a choice of catalyst between Pt–Co/ $\text{Al}_2\text{O}_3$  and Mn–Pt–Co/ $\text{Al}_2\text{O}_3$  and the presence or absence of a hydrocracker. In each case, two main criteria were analyzed: the product distributions, fuel specifications, amount of on-spec. distillate produced, and power production (MW).

The fixed variables for all conversions in this evaluation are shown in Table 3. Variables that were altered in each scenario to maintain on-spec. distillate properties include the temperatures of the flash tanks in the product recovery and refining section as well as the reboiler duty, distillation column feed temperature and side stream flowrate. The optimization of each of these units is shown in the ESI.†

### Product distributions

At the base case conversion of  $X_{\text{CO}} = 60\%$  with a Pt–Co/ $\text{Al}_2\text{O}_3$  catalyst, the chain growth probability for the Fischer–Tropsch synthesis is high, and thus the hydrocarbon product distribution is wide with significant amounts of both naphtha, distillate and waxes. The Fischer–Tropsch product spectrum is, however, significantly affected by CO conversion, catalyst, and reaction conditions. Fig. 9 shows the Fischer–Tropsch carbon number distributions of the product obtained over the two catalysts (Pt–Co/ $\text{Al}_2\text{O}_3$  and Mn–Pt–Co/ $\text{Al}_2\text{O}_3$ ) in a slurry bed reactor at 20 bar and  $220\text{ }^\circ\text{C}$  operating at conversions between  $X_{\text{CO}} = 60$  and  $X_{\text{CO}} = 90\%$  based on empirical data.<sup>15,19</sup>

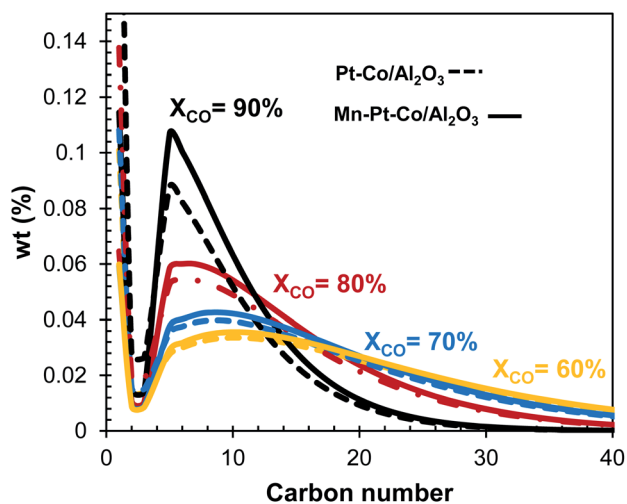


Fig. 9 Carbon number distribution for Pt–Co/ $\text{Al}_2\text{O}_3$  and Mn–Pt–Co/ $\text{Al}_2\text{O}_3$  in a slurry bed reactor at various conversions based on data from ref. 15 and 19.

**Conversion effects.** At a conversion of  $X_{\text{CO}} = 60\%$ , the product distribution is wide for both catalysts, with a significant portion of hydrocarbons in the  $\text{C}_{22+}$  wax range. Increasing the conversion to  $X_{\text{CO}} = 70\%$  and  $X_{\text{CO}} = 80\%$ , decreases the width of the product distribution, and shifts it towards lighter hydrocarbons, due to lower chain growth probabilities. This shift is even more pronounced at  $90\%$  conversion, where almost no  $\text{C}_{30+}$  hydrocarbons seem to be formed. As high conversion result in less wax production ( $\text{C}_{22+}$ ), a hydrocracker may not be strictly necessary to enhance diesel yields at these conditions, whilst hydrocracking is critical for systems operating at low conversion.

**Catalyst choice.** The product selectivity is affected by conversion, described in detail elsewhere,<sup>15</sup> and going to a high conversion includes a shift from olefinic to paraffinic hydrocarbons, a strong increase in methane and carbon dioxide selectivity and a decrease in  $\text{C}_{5+}$  yield (see Fig. 2 and 4). The significant negative effects of conversion on the selectivity of the Fischer–Tropsch synthesis at high conversion necessitate a dedicated catalyst for single-pass systems.

Promoting cobalt-based catalysts with manganese is one method to enhance selectivity towards  $\text{C}_{5+}$  at high conversion.<sup>16,19</sup> Using a Mn : Co ratio of 0.15 mol/mol, the selectivity for the formation of  $\text{CO}_2$  and  $\text{CH}_4$  have been shown to decrease by up to 6 C-% and 12 C-% respectively at  $X_{\text{CO}} = 90\%$ .<sup>9,19</sup> Changing the catalyst from Pt–Co/ $\text{Al}_2\text{O}_3$  to Mn–Pt–Co/ $\text{Al}_2\text{O}_3$  has little effect on the overall product distribution at lower conversions (see Fig. 9). However, operating the Fischer–Tropsch synthesis at  $X_{\text{CO}} = 80\%$  and  $X_{\text{CO}} = 90\%$  with the manganese promoted catalyst appears to significantly increase the fraction of hydrocarbons within the naphtha and diesel range. Changing the catalyst from Pt–Co/ $\text{Al}_2\text{O}_3$  does not significantly affect the mean and the shape of the product distribution (*i.e.* chain growth probability in the fraction of long-chain hydrocarbons), but rather fraction of hydrocarbons in the  $\text{C}_{5+}$ -range as manganese as a promoter primarily reduces the selectivity for the formation of methane at a given conversion. Thus, developing a dedicated catalyst for high conversion could enable much higher yields for the overall process.

**Process conditions.** The empirical data used for this evaluation were based on selectivity data using Pt–Co/ $\text{Al}_2\text{O}_3$  and Mn–Pt–Co/ $\text{Al}_2\text{O}_3$  in a slurry bed reactor at 20 bar and  $220\text{ }^\circ\text{C}$ . The Fischer–Tropsch synthesis could, however, be operated at a higher pressure, *e.g.*, 30 bar, without requiring an additional compressor (albeit with higher compression energy requirements). These process conditions will inevitably affect the Fischer–Tropsch product selectivity. Increasing the reaction pressure within the Fischer–Tropsch synthesis is known to increase the chain growth probability and decrease methane selectivity.<sup>52,53</sup> This would be particularly attractive at high conversion ( $X_{\text{CO}} = 80\text{--}90\%$ ) where methane selectivity is significant (see Fig. 4), and a shift from the naphtha to diesel range (see Fig. 9) would significantly increase overall carbon yields.

**Hydrocracking.** Fig. 10 shows the carbon number distribution of the hydrocarbons in the products coming from the



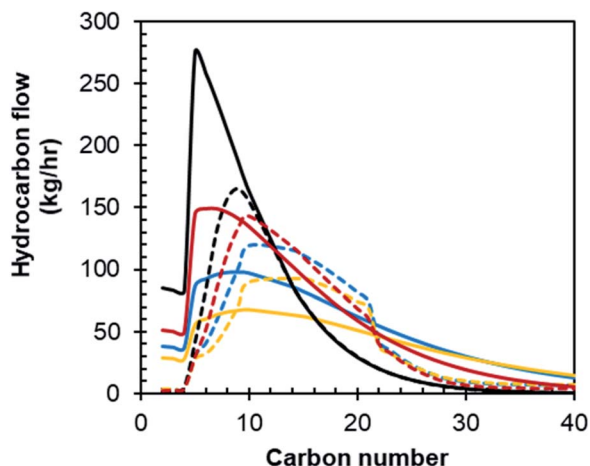


Fig. 10 The hydrocarbon distribution of the products from the Fischer-Tropsch reactor (—) and the hydrocarbon distribution of the feed to the atmospheric distillation column incl. the hydrocracking product (---) for a feed generated by operating the Fischer-Tropsch synthesis at a conversion of ● 60%, ● 70%, ● 80%, ● 90%.

Fischer-Tropsch reactor and the combined feed to the distillation column after hydrocracking. As there was a decrease in Fischer-Tropsch wax products with increasing conversion (due to decreasing alpha values), the improvement of the distillate

yield after hydrocracking decreased accordingly. For a conversion of  $X_{CO} = 60\%$ ,  $70\%$ ,  $80\%$  and  $90\%$  in the Fischer-Tropsch synthesis, the  $C_{10}$ - $C_{22}$  distillate yield was improved by 40%, 28%, 12% and 0.6% due to hydrocracking, respectively. This clearly demonstrates that, based on the improvement of the yield, the hydrocracker can only be justified if the conversion of CO in the Fischer-Tropsch synthesis is limited.

It should be noted, however, that the *Decentralized Diesel* plant operates with a well-mixed Fischer-Tropsch reactor (slurry-bed reactor) which, at high conversion, contributes to the shift of the product distribution towards lighter products reducing the wax production. A hydrocracker may be needed when using reactors with less back-mixing (packed bed reactor, slurry bubble columns) for the Fischer-Tropsch synthesis as the product is a result of all different conditions in the reactor. Hence, the necessity of a hydrocracker must be considered together with type of Fischer-Tropsch reactor chosen for the specific application.

### Fuel specifications

Fig. 11 shows the optimized carbon-number distribution of the distillate (withdrawn from the side stream of the atmospheric distillation column) for a conversion of (a) 60%, (b) 70%, (c) 80% and (d) 90% in the Fischer-Tropsch synthesis obtained over an Pt-Co/ $Al_2O_3$  catalyst, whilst having a hydrocracking unit

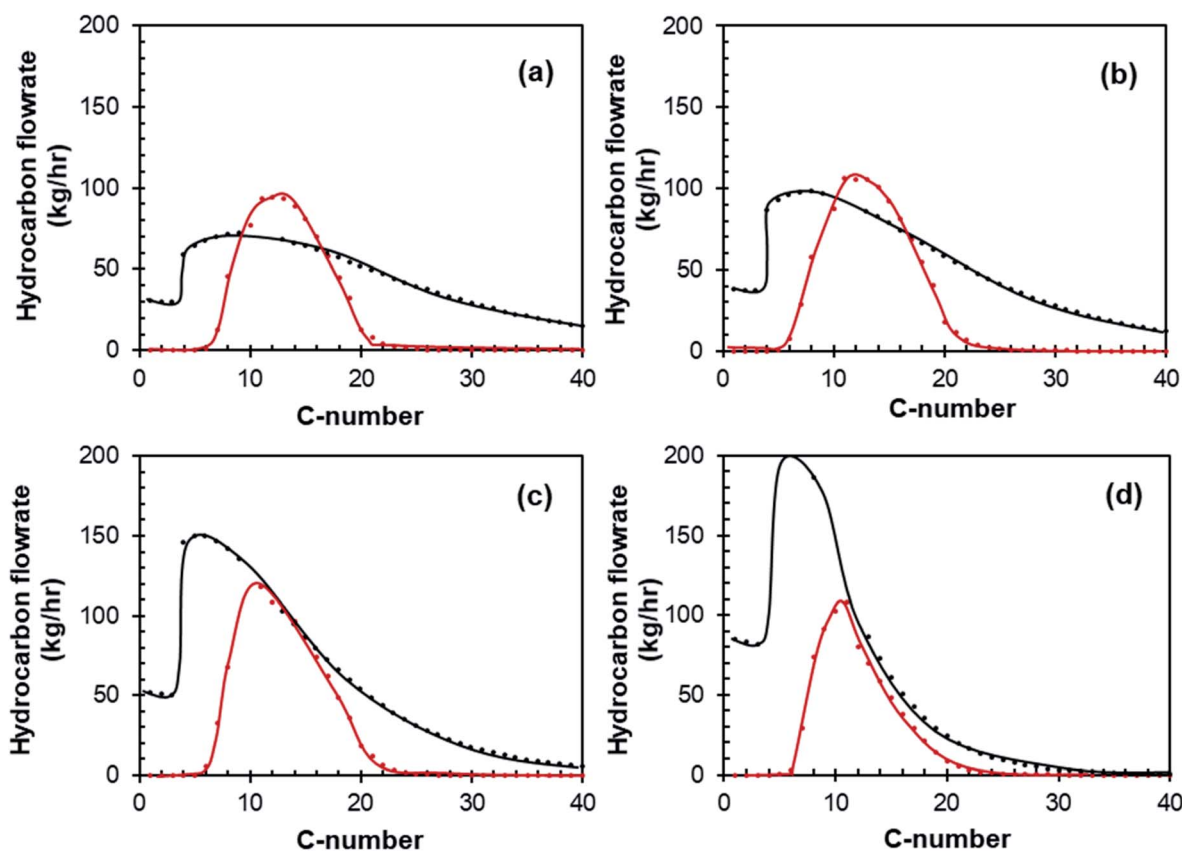


Fig. 11 Mass hydrocarbon distribution  $C_2$  to  $C_{40}$  product compounds for — Fischer-Tropsch products and — distillate product for  $X_{CO} =$  (a) 60%, (b) 70%, (c) 80% and (d) 90% for Pt-Co/ $Al_2O_3$  for the case with a hydrocracker.



Table 4 Specifications of fuel produced in the optimized case for Pt-Co/Al<sub>2</sub>O<sub>3</sub> with a hydrocracker

	ASTM D975:15b (US)	EN 590:2014 (EU) <sup>55</sup>	AFRI-5:2016 (AU) <sup>56</sup>	SANS 342:2016 (ZA) <sup>57</sup>	CO Conversion			
					60%	70%	80%	90%
Diesel density at 15 °C	— <sup>a</sup>	820	820–880	805–850	743	741	740	741
Water, ppm	500	200	— <sup>a</sup>	250	3	52	24	9.6
Cetane number min	49	51	49	51	91	90	90	89
Viscosity at 40 °C mm <sup>2</sup> s <sup>-1</sup>	1.9–4.1	2.0–4.5	— <sup>a</sup>	2.2–5.3	2.5	2.3	2.0	1.9
Flash point, °C	55	55	— <sup>a</sup>	— <sup>a</sup>	67	60	60	67
Cloud point, °C	≤5, ≤34 <sup>b</sup>	≤10, ≤34 <sup>b</sup>	— <sup>a</sup>	+6	–11	–17	–30	–35
Distillation								
T <sub>95</sub>	370	360	— <sup>a</sup>	362	350	355	360	350
T <sub>90</sub>	338			360	335	337	337	330

<sup>a</sup> No limit specified. <sup>b</sup> Severe winter and arctic grade.

in the overall process. Increasing the conversion in the Fischer-Tropsch synthesis from 60% to 90% resulted in a narrower product distribution, with a mean shifted to lower carbon numbers.

The specifications of the fuel produced (side stream distillate) in the optimized cases for  $X_{CO}$  from 60% to 90% obtained over a Pt-Co/Al<sub>2</sub>O<sub>3</sub> catalyst are shown in Table 4. For each case, the yield was optimized whilst trying to stay within the limits of diesel specifications. The optimized distillate distribution was limited by the flash point on the lighter end and the distillation profile on the heavier end.

Fischer-Tropsch LTFT distillate typically has a high cetane number in relation to typical crude-oil derived diesel. This is true for this process, as can be seen by 4, where the cetane number for all cases is *ca.* 90, as opposed to the specifications which are between 49 and 51.<sup>47</sup>

The water content in the distillate is between 3 and 52 ppm, far below the specifications between 200 and 500 ppm (see Table 4). The water content of the distillate is determined by the choice of reboiler duties and feed temperatures (see Table 3) which were adjusted slightly in each case to ensure distillation profiles and flash point temperatures were within spec. The effect of these changes on the distribution of carbon in the distillate is shown in ESI Fig. S-9.†

A typical issue for LTFT diesel is the cloud point – which represents the temperature at which diesel forms a cloudy appearance due to the waxy hydrocarbons beginning to solidify. This specification is set to avoid blockages in fuel filters and engine injectors. It is inherently based on the minimum temperatures within a region. This specification can vary significantly between 6 °C (South Africa) and –34 °C (severe weather specification in EU and US). Africa has no cloud point specification. Cloud points for the distillate stream were determined using a correlation<sup>50</sup> that takes into account the specific gravity,  $T_{10\%}$ ,  $T_{50\%}$  and  $T_{90\%}$ . The cloud point for distillate produced by the case with a Fischer-Tropsch conversion of  $X_{CO} = 60\%$  and a Pt-Co/Al<sub>2</sub>O<sub>3</sub> catalyst is –11 °C. This only narrowly meets the normal specifications for the EU and US (–10 °C and –5 °C respectively), albeit is firmly within the South African specifications. The cloud point decreases with increasing CO conversion, as the amount of wax produced in

the Fischer-Tropsch synthesis decreases. Most of the cases (all except for  $X_{CO} = 90\%$ ) do not meet the requirement for severe or arctic weather. Thus, distillate produced by this process may need to undergo isomerization for extreme cold conditions, however for Sub-Saharan Africa this is not necessary.

The specification that LTFT distillate often cannot meet, and the distillate from this process does not meet, is density. The distillate product from this process has a density of *ca.* 740 kg m<sup>-3</sup>, far below the 780 kg m<sup>-3</sup> specification for the EU (EN 590), African (AFRI-5) or South African (SANS 342:2016) specifications.<sup>54</sup> United States of America (ASTM D975) has no such specification. Thus, depending on the region, the distillate produced from this process may require blending with crude oil derivatives, or higher density blending material, to be legally sold on the diesel market.

The viscosity of the distillate produced falls between 2.5 and 1.9 for CO conversions  $X_{CO} = 60\%$  to  $X_{CO} = 90\%$ . This is on the lower end of the viscosity range, with  $X_{CO} > 80\%$  falling out of spec. for South Africa, and  $X_{CO} = 90\%$  falling out of spec. for the EU and South Africa. All cases fall within specifications for the US. The viscosity, like density, may be improved by blending.

### Fuel yield

From each of the 16 optimized scenarios, the overall fuel production was calculated (see Fig. 12). For a Pt-Co/Al<sub>2</sub>O<sub>3</sub> catalyst with hydrocracking, a conversion of  $X_{CO} = 60\%$  in the Fischer-Tropsch synthesis resulted in a production rate of distillate of 183 bbl per day. This is equivalent to an overall carbon yield (incl. carbon dioxide) of distillate of 14 C% (Table 5). Increasing the conversion in the Fischer-Tropsch synthesis unit increased the distillate production rate up to a maximum of 232 bbl per day (overall carbon yield of 16 C-%) at *ca.*  $X_{CO} = 75\%$ . The distillate production rate then dropped off sharply as the conversion was increased to  $X_{CO} = 90\%$ , obtaining only 142 bbl per day (overall carbon yield of 11 C-%). The sharp drop-off in the production rate (and overall carbon yield) upon increasing the conversion to 90% is a consequence of the shift in the product selectivity in the Fischer-Tropsch synthesis over Pt-Co/Al<sub>2</sub>O<sub>3</sub> operating at 220 °C and 20 bar; at these conditions, the selectivity for the formation of methane and for the



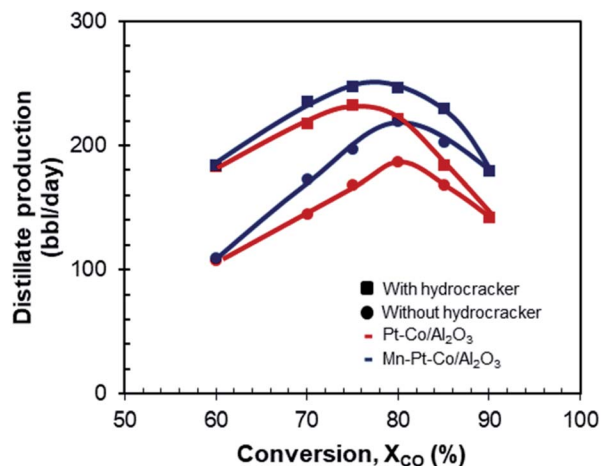


Fig. 12 Distillate production as a function of conversion for Pt–Co/Al<sub>2</sub>O<sub>3</sub> and Mn–Pt–Co/Al<sub>2</sub>O<sub>3</sub> with and without hydrocracking.

Table 5 Refining and overall yield of distillate range product for the optimised version of each case

Catalyst	Overall carbon yield of distillate from biogas (C-%)	Conversion			
		60%	70%	80%	90%
Pt–Co/Al <sub>2</sub> O <sub>3</sub>	With hydrocracker	14	16	16	11
	Without hydrocracker	8	10	14	11
Mn–Pt–Co/Al <sub>2</sub> O <sub>3</sub>	With hydrocracker	14	17	18	13
	Without hydrocracker	8	12	16	13

formation of CO<sub>2</sub> increases dramatically<sup>15</sup> and thus reducing the selectivity for the formation of liquid hydrocarbons.

Operating the process with a Pt–Co/Al<sub>2</sub>O<sub>3</sub> Fischer–Tropsch catalyst without a hydrocracker resulted in significantly less distillate, especially when operating the Fischer–Tropsch synthesis at lower conversions (whilst at the same time increasing the production of wax). This effect was most significant at  $X_{CO} = 60\%$  (109 bbl per day, 8 C-% yield). The best conversion for distillate yield in this case was shifted from  $X_{CO} = 75\%$  to  $X_{CO} = 80\%$  with a production of only 186 bbl per day (14 C-% yield). Past this maximum there was also a strong decrease in productivity, reducing to 142 bbl per day at  $X_{CO} = 90\%$ , equal to the case of using a Pt–Co/Al<sub>2</sub>O<sub>3</sub> catalyst in conjunction with a hydrocracker in the design. This confirmed that, for very high conversions, a hydrocracker can be redundant due to the change in product distribution (see Fig. 9 and 10).

The manganese-promoted catalyst Mn–Pt–Co/Al<sub>2</sub>O<sub>3</sub> seemed to produce roughly equal amounts of distillate as its unmodified counterpart for the lower conversion in the Fischer–Tropsch synthesis of  $X_{CO} = 60\%$  (183 bbl per day and 109 bbl per day for case with and without hydrocracking respectively). On increasing the conversion, however, promotion with manganese seemed to have a progressively more significant effect on distillate production rate. At conversions of 70%, 80% and 90% in the Fischer–Tropsch synthesis, the distillate

production was 235, 246 and 179 bbl per day respectively which represented a relative improvement over the unmodified Pt–Co/Al<sub>2</sub>O<sub>3</sub> of 8%, 12% and 25% respectively for the case with a hydrocracker. The productivity over the manganese-promoted catalyst was less influenced by the change in conversion than the unmodified catalyst. As a result, this system would be less sensitive to shifts in conversion due to external disturbances. These results emphasize the need for catalysts that have been specifically designed to work at high conversion in order to further enhance distillate fuel yields.

Operating Mn–Pt–Co/Al<sub>2</sub>O<sub>3</sub> in a system without a hydrocracker, decreased the distillate production significantly at low conversion, with an insignificant effect when moving to  $X_{CO} = 90\%$ . Nevertheless, it seems advisable to operate the manganese promoted catalyst at a conversion of  $X_{CO} = 80\%$  in combination with a hydrocracker to maximize the diesel yield (overall carbon yield of 18 C-%) and production rate (246 bbl per day).

The process as it stands has a very low carbon yields, even at optimally high conversions. Overall carbon yields range from 8 C-% to 18 C-%, which is consistent with the carbon flow diagram for the base case shown in Fig. 7. This is equivalent to a carbon yield from methane of 11 C-% to 24 C-%.

There are several explanations for the low carbon yields seen in this study. Firstly, the very low (net negative) conversion of CO<sub>2</sub> in the tri-reformer resulted in a loss of yield of approximately 25 C-% at the start of the process. This CO<sub>2</sub> acts as an inert throughout the rest of the process, including the power plant where it eventually leaves as stack gas. Secondly, even with an improved catalyst, the Fischer–Tropsch reactor only produced a fraction within the distillate carbon range, with significant amounts of carbon lost into the wax and naphtha fractions. Finally, a portion of the distillate is lost through the bottoms of the atmospheric distillation column.

The low yield of this process is a direct result of the design choices and philosophy for this process and should be contextualized with regards to the purpose of the design. In the classical coal-to-liquid process, the objective is to get as much carbon as possible into desired products, whilst at the same time minimizing energy losses. This means that, for CTL, the product spectrum can be quite diverse with significant recycling and refining requirements. In the case of this design, the primary objective is to convert biogas from organic waste to minimize methane emissions and to enable the creation of energy from localized feedstock in a decentralized, off-grid, manner. The different objectives result in a different design approach and significantly different product spectrum. The *Decentralized Diesel* design prioritizes simplicity, capital cost efficiency and energy self-sufficiency over carbon efficiency.

There are ways to significantly enhance carbon yields by changing the design, albeit these would naturally require trade-offs.

**Converting CO<sub>2</sub> conversion in reformer.** The formation of CO<sub>2</sub> in the tri-reformer (as opposed to conversion of CO<sub>2</sub>) is directly linked to the choice of reforming conditions and feeds chosen for this process (see ESI Fig. S-1†). One of the key design constraints for the *Decentralized Diesel* system the requirement to operate with energy self-sufficiency. This meant that the



reforming step was required to operate under autothermal conditions. The only way to achieve this is through tri-reforming (reforming of biogas with steam and oxygen). Whilst this means that no energy needs to be added to the system, it has the negative effect of diluting syngas with nitrogen (from air) and a negative CO<sub>2</sub> conversion.

Dry reforming involves the conversion of CH<sub>4</sub> and CO<sub>2</sub> to CO and H<sub>2</sub>. This reaction yields higher conversions of CO<sub>2</sub> (ref. 58) and eliminates gas dilution from nitrogen. However, as dry reforming is endothermic, the system would require external heating. Another issue of dry reforming would be the high levels of carbon deposition (coking) on the surface of the catalyst,<sup>24</sup> which would need to be regenerated online in order to avoid constant replacement and downtime. Furthermore, dry reforming results in low H<sub>2</sub>/CO ratios between 0.5–1.5.<sup>59</sup> This requires extensive water-gas shift to further correct for the H<sub>2</sub>/CO ratio (2), if cobalt is to be used as a Fischer–Tropsch catalyst.

To enable conversion of carbon dioxide within the reformer itself, the system requires external heating, catalyst regeneration and a far larger water–gas shift reaction system (or a change from cobalt to iron catalyst). However, if dry reforming was used, and energy could be added to the system, then various factors can be improved:

- Enhanced conversion of CO<sub>2</sub> in the reformer by operating the system without a flow of air.
- Less nitrogen in the Fischer–Tropsch reactor which dilutes the system, decreasing rates.
- Increased partial pressures in the Fischer–Tropsch reactor which will improve selectivities.

**Increasing C<sub>10</sub>–C<sub>22</sub> fraction.** Even with a catalyst that can operate ideally under high conversion conditions, and an optimal Fischer–Tropsch conversion, the amount of diesel range hydrocarbons (C<sub>10</sub>–C<sub>22</sub>) produced in the Fischer–Tropsch synthesis is still low. This can be improved in several ways.

- Increase pressure to shift the product distribution to higher carbon numbers. This may increase the carbon fraction of distillate substantially, especially at higher conversions. However, this will likely require additional compressors after the reformer as the compression ratio increases. This may also further increase capital cost and energy requirements of the process and may, depending on the pressure, mean the process is no longer energy self-sufficient.

• Decrease dilution factor in the Fischer–Tropsch synthesis by including an air separation unit. If pure oxygen was used in the reformer the partial pressures of syngas in the process would increase, improving the rate as well as the yield of distillate at higher conversions (increased partial pressures of CO and H<sub>2</sub> results in increased chain growth probability). The air-separation unit is, however, capital- and compression-intensive and may limit the ability of the plant to operate in a decentralized, off-grid manner.

- Catalyst development that focuses on the *in situ* hydrocracking of long chain hydrocarbons could enhance the amount of C<sub>10</sub>–C<sub>22</sub> range hydrocarbons produced, whilst a catalyst that can facilitate the hydrogenation of CO<sub>2</sub> within the Fischer–Tropsch reactor may enhance carbon utilization.

• A different Fischer–Tropsch reactor (fixed bed or micro) may minimize the effects of high conversion by limiting the high partial pressure of water, and low partial pressure of CO and H<sub>2</sub>, to a smaller part of the catalyst bed. This comes with a trade-off of more complex heat transfer and less straightforward catalyst replacement.

**Refining efficiency.** As the purpose of this design was only to refine one singular product, to the specifications required for distillate, a significant fraction of carbon is used for power production, or leaves a heavier wax fraction, rather being produced as diesel fuel. In reality, the latter could be solved by a liquid recycle from the bottoms of the atmospheric distillation column to the hydrocracker, which was not modelled in this study (however, from a purely engineering perspective this could be easily implemented).

### Power generation

Fig. 13 shows the effect of conversion on the gross and net power generation for the design with the Fischer–Tropsch synthesis over Pt–Co/Al<sub>2</sub>O<sub>3</sub> or Mn–Pt–Co/Al<sub>2</sub>O<sub>3</sub> -catalyst, and with or without a hydrocracking unit. The net power generation was calculated after accounting for the power required to run the three compressors in the syngas generation section as well as the hydrogen compressor (only for scenarios with hydrocracking) and the water pumps (pressures as per Table 3).

The conversion in the Fischer–Tropsch synthesis, rather than the type of catalyst or the presence or absence of a hydrocracker had the most significant effect on the amount of power generated. At a lower conversion of X<sub>CO</sub> = 60% the gross power generated ranged from 7.9 MW to 8.5 MW, with Pt–Co/Al<sub>2</sub>O<sub>3</sub> producing only slightly more. The net power generation at this conversion was between 2.4 and 3 MW. As the conversion increases, the amount of power generated decreased in all cases, reaching a minimum at X<sub>CO</sub> = 80%. The gross and net power production increased significantly at X<sub>CO</sub> = 90% to 8.7–9.6 MW and 3.2–4.2 MW respectively in all cases. The poorer selectivity towards long-chain hydrocarbons in the Fischer–Tropsch synthesis over the Pt–Co/Al<sub>2</sub>O<sub>3</sub> catalyst in comparison

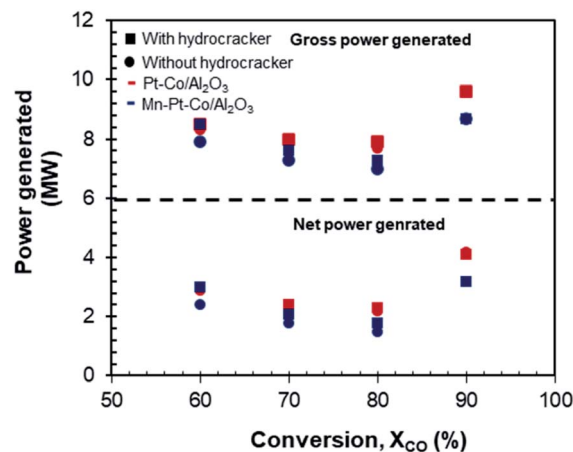


Fig. 13 Power generated as a function of conversion for Pt–Co/Al<sub>2</sub>O<sub>3</sub> and Mn–Pt–Co/Al<sub>2</sub>O<sub>3</sub> with and without hydrocracking.



Table 6 Lower heating values of reactants and products (MW) as well as power generated as a function of conversion

CO conversion (%)	Lower heating value reactants (MW)	Lower heating value of products (MW)			Power generated (MW)
		Tail gas	Distillate	Wax	
60	67	36	5.3	2.1	8.5
70	67	34	8.4	1.5	8
80	67	33	9.1	1.5	7.9
90	67	39	6.3	0.6	9.6

Table 7 Energy efficiencies of the tri-reforming/Fischer–Tropsch process, power plant and overall process

CO conversion (%)	Energy efficiency (%)			
	Fischer–Tropsch process <sup>a</sup>	Power plant (gross) <sup>b</sup>	Overall (gross) <sup>c</sup>	Overall (net) <sup>d</sup>
60	66	23	24	16
70	66	23	27	18
80	65	24	28	19
90	69	25	25	17

<sup>a</sup> LHV of tail gas, distillate and wax relative to LHV of biogas. <sup>b</sup> Gross power generated relative to LHV of tail gas. <sup>c</sup> LHV of distillate and wax as well as power generated (gross) (MW) relative to LHV of biogas. <sup>d</sup> LHV of distillate and wax as well as power generated (net) (MW) relative to LHV of biogas.

to the selectivity obtained over the manganese promoted catalyst results in a larger tail gas stream and hence increased power generation across the conversion range, but especially at high conversion where the performance difference between the catalysts was more substantial.

### Energy efficiency

Table 6 shows the LHV for the reactants and products for conversions 60–90% as well as the gross electricity generated. The LHV of the tail gas, distillate, and wax ranges from 33–39 MW, 5.3–9.1 MW and 0.6–2.1 MW. The difference in the LHV of products is a function of the amount of each product formed rather than the energy density, with  $X_{CO} = 80\%$  having the highest LHV for distillate and  $X_{CO} = 90\%$  having the highest LHV for tail gas (with thus translates to the highest electricity generated).

Table 7 shows the subsequent energy efficiencies of the Fischer–Tropsch process, power plant and overall, for each conversion. The efficiencies do not change significantly with conversion, ranging from 66–69% (Fischer–Tropsch process), 23–25% for power plant (gross power generated) and 24–28% overall. If net power generated is considered (*i.e.*, after power used for compressors and pumps are accounted for) thus satisfying the off-grid requirement, the net efficiency of the overall process is between 16–19%. These are low energy efficiencies when compared to typical steam turbine systems.

This is primarily due to the strong dilution factor ( $N_2$  and  $CO_2$ ) in the feed, as well as the fact that not all the heat from the flu gas was able to be recovered (albeit this can be used in plant-wide heat integration which was not implemented at this stage).

The dilution factor may be decreased if an air-separation unit was included in the design. However, this would require extensive compression across the plant (including in the air-

separation plant itself), which would require significant energy from the power plant, thus potentially decreasing the energy self-sufficient requirement.

## Conclusions

A single pass Fischer–Tropsch biogas-to-diesel plant producing on-spec distillate fuel from methane-rich biogas was evaluated using Aspen® Simulation Workbook. The purpose of the evaluation of was to determine the effect of Fischer–Tropsch conversion, type of catalyst and refining configuration on the yield and efficiency of the process. The evaluation consisted of 16 scenarios, including four Fischer–Tropsch conversions (60%, 70%, 80% and 90%), two Fischer–Tropsch catalysts (Pt–Co/ $Al_2O_3$  and Mn–Co/ $Al_2O_3$ ) and a partial refining plant with and without hydrocracking. Overall carbon yields for the on-spec distillate were found to be low in all cases (between 8 C-% and 18 C-%). This was due to low  $CO_2$  conversions in the tri-reformer, low yields to  $C_{10}$ – $C_{22}$  in the Fischer–Tropsch reactor and a loss of distillate into the wax fraction of the distillation column. The latter may be remediated by recycling the liquid back to a hydrocracker. The low carbon yield is a result of the design philosophy which prioritized simplicity and energy self-sufficiency over carbon efficiency. The purpose of the design, as opposed to standard CTL installations, is to reducing methane emissions and generating energy in remote regions. Improvements to the carbon yield can be made, albeit each with a tradeoff. By using non-autothermal dry reforming to enhance  $CO_2$  conversion and decrease gas dilution, energy addition is required. To improve  $C_{10}$ – $C_{12}$  yields, the Fischer–Tropsch reaction could be operated at higher pressure, or an air-separation unit (to provide pure oxygen) could be used prior to reforming, albeit both would increase compression requirements, energy intensity and capital costs.



The tail gas from the biogas-to-distillate plant was used to generate power with a gross generation of between 7 MW and 9.6 MW and a net generation (after compressors and pumps) of between 1.8 and 4.2 MW. The amount of power generated was strongly affected by conversion, whilst the type of Fischer-Tropsch catalyst and presence or absence of a hydrocracker had only a small effect.

The optimal case was found to be a Mn-Co/Al<sub>2</sub>O<sub>3</sub> operated at X<sub>CO</sub> = 80% with a hydrocracker. The on-spec overall distillate yield for this case was 18 C-%, at a production rate of 246 bbl per day. The power produced by this case was 7.3 MW gross and 1.8 MW net, with an overall energy efficiency (gross) of 28%. It is thus important to design catalysts specific for operating the Fischer-Tropsch process at high conversions.

This study shows that a single Fischer-Tropsch biogas-to-distillate plant that is self-sustaining is feasible from a process and catalytic perspective, especially when higher conversions and catalyst improvements for high conversion (in this case *via* manganese promotion) are incorporated.

## Conflicts of interest

There are no conflicts to declare.

## Acknowledgements

The scientific guidance from Prof. Arno de Klerk is gratefully acknowledged. Funding from Sasol Ltd, Queen Elizabeth Diamond Jubilee Scholarship and L'Oréal for Women in Science. This research was in part supported by the South African Research Chair Initiative (SARChI), UID 114606, and the BRICS-program, (BRIC160624174073; UID 110487)

## Notes and references

- M. Marchese, S. Chesta, M. Santarelli and A. Lanzini, *Energy*, 2021, **228**, 120581.
- M. Martinelli, M. K. Gnanamani, S. LeViness, G. Jacobs and W. D. Shafer, *Appl. Catal., A*, 2020, **608**, 117740.
- M. Shahabuddin, M. T. Alam, B. B. Krishna, T. Bhaskar and G. Perkins, *Bioresour. Technol.*, 2020, **312**, 123596.
- V. Arutyunov, A. Nikitin, L. Strekova, V. Savchenko and I. Sedov, *Catal. Today*, 2020, **379**, 23–27.
- X. Zhao, A. Naqi, D. M. Walker, T. Roberge, M. Kastelic, B. Joseph and J. N. Kuhn, *Sustainable Energy Fuels*, 2019, **3**, 539–549.
- H. Boerrigter, *Economy of Biomass-to-Liquids (BTL) plants: An engineering assessment*, Energy Research Centre of the Netherlands, Report ECN-C-06-019, 2006.
- V. Shah, N. J. Kuehn and M. J. Turner, Cost and performance baseline for fossil energy plants, in *Coal-to-liquids via Fischer-Tropsch synthesis*, United States, 2014, vol. 4, <https://www.netl.doe.gov/energy-analysis/details?id=736>, accessed June 2017.
- D. J. Wilhelm, D. R. Simbeck, A. D. Karp and R. L. Dickenson, *Fuel Process. Technol.*, 2001, **71**, 139–148.
- C. L. Tucker, PhD thesis, University of Cape, Town, South Africa, 2020.
- C. L. Tucker and E. van Steen, in *Chemical approaches for management of solid waste*, CRC Press, Taylor and Francis Group, Florida, 2020 (in review).
- Bechtel, *Aspen process flowsheet simulation model of a battelle biomass-based gasification, Fischer-Tropsch liquefaction and combined-cycle power plant*, Report for U.S Department of Energy, 1998.
- G. N. Choi, S. J. Kramer, S. S. Tam and J. M. Fox, *Design/economics of a once-through natural gas Fischer-Tropsch plant with power co-production*, Bechtel Corporation, 1996.
- M. Ostadi, K. Dalane, E. Rytter and M. Hillestad, *Fuel Process. Technol.*, 2015, **139**, 186–195.
- B. Liu, S. Geng, J. Zheng, X. Jia, F. Jiang and X. Liu, *ChemCatChem*, 2018, **10**, 4718–4732.
- C. L. Tucker and E. van Steen, *Catal. Today*, 2020, **342**, 115–123.
- Y. Jiang, H. Wang, S. Li, C. Yang, L. Zhong, P. Gao and Y. Sun, *Ind. Eng. Chem. Res.*, 2020, **59**, 8195–8201.
- W. Ma, G. Jacobs, Y. Ji, T. Bhatelia, D. B. Bukur, S. Khalid and B. H. Davis, *Top. Catal.*, 2011, **54**, 757–767.
- D. B. Bukur, Z. Pan, W. Ma, G. Jacobs and B. H. Davis, *Catal. Lett.*, 2012, **142**, 1382–1387.
- C. L. Tucker and E. van Steen, *Manganese promotion of Pt-Co/Al<sub>2</sub>O<sub>3</sub> catalyst for the single pass Fischer-Tropsch biomass-to-liquid operation*, North American Catalysis Society Meeting, 2019.
- O. C. David, D. Gorri, A. Urriaga and I. Ortiz, *J. Membr. Sci.*, 2011, **378**, 359–368.
- D. Leckel and M. Liwanga-Ehumbu, *Energy Fuels*, 2006, **20**, 2330–2336.
- GreenCape, *Waste Economy: Market Intelligence Report* 2015, pp. 1–55.
- D. Hoornweg and B. Perinaz, *What a Waste a global review of solid waste management*, 2012.
- S. A. Chattanathan, S. Adhikari, M. McVey and O. Fasina, *Int. J. Hydrogen Energy*, 2014, **39**, 19905–19911.
- A. Hilkiah Igoni, M. J. Ayotamuno, C. L. Eze, S. O. T. Ogaji and S. D. Probert, *Appl. Energy*, 2008, **85**, 430–438.
- A. Naqi, Ms thesis, University of South Florida, USA, 2018.
- K. Aasberg-Petersen, T. S. Christensen, C. Stub Nielsen and I. Dybkjær, *Fuel Process. Technol.*, 2003, **83**, 253–261.
- C. Song and W. Pan, *Catal. Today*, 2004, **98**, 463–484.
- N. Kumar, M. Shojaee and J. J. Spivey, *Curr. Opin. Chem. Eng.*, 2015, **9**, 8–15.
- S. G. Gopaul and A. Dutta, *Int. J. Hydrogen Energy*, 2015, **40**, 6307–6318.
- X. Zhao, H. T. Ngo, D. M. Walker, D. Weber, D. Maiti, A. D. Petrov, B. Joseph and J. N. Kuhn, *Chem. Eng. Commun.*, 2018, **205**, 1–37.
- P. S. Roy, A. S. K. Raju and K. Kim, *Fuel*, 2015, **139**, 314–320.
- A. I. Tsyganok, M. Inaba, T. Tsunoda, K. Suzuki, K. Takehira and T. Hayakawa, *Appl. Catal., A*, 2004, **275**, 149–155.
- H. S. Roh, K. Y. Koo, U. D. Joshi and W. L. Yoon, *Catal. Lett.*, 2008, **125**, 283–288.



- 35 M. M. B. Noureldin, N. O. Elbashir and M. M. El-Halwagi, *Ind. Eng. Chem. Res.*, 2014, **53**, 1841–1855.
- 36 B. H. Davis and M. L. Occelli, *Fischer-Tropsch Synthesis, Catalysts, and Catalysis*, CRC Press, Taylor and Francis Group, Florida, 2016.
- 37 R. Y. Chein and W. H. Hsu, *Energies*, 2018, **11**, 1–18.
- 38 C. M. Kalamaras, P. Panagiotopoulou, D. I. Kondarides and A. M. Efstathiou, *J. Catal.*, 2009, **264**, 117–129.
- 39 H. Iida and A. Igarashi, *Appl. Catal., A*, 2006, **298**, 152–160.
- 40 S. S. Hosseini, M. M. Teoh and T. S. Chung, *Polymer*, 2008, **49**, 1594–1603.
- 41 Y. Zhang, I. H. Musselman, J. P. Ferraris and K. J. Balkus, *J. Membr. Sci.*, 2008, **313**, 170–181.
- 42 F. Weigelt, P. Georgopoulos, S. Shishatskiy, V. Filiz, T. Brinkmann and V. Abetz, *Polymers*, 2018, **10**(1), 51.
- 43 D. Edlund, in *Hydrogen and Syngas Production and Purification Technologies*, 2010, pp. 357–384.
- 44 F. G. Botes, B. van Dyk and C. McGregor, *Ind. Eng. Chem. Res.*, 2009, **48**, 10439–10447.
- 45 C. L. Tucker, E. van Steen and M. Claeys, *Catal. Sci. Technol.*, 2020, **10**(20), 7056–7066.
- 46 A. De Klerk, *Fischer-Tropsch refining*, John Wiley & Sons, 2012, pp. 1–601.
- 47 M. E. Dry, *J. Chem. Technol. Biotechnol.*, 2002, **77**, 43–50.
- 48 ASTM International, *ASTM D93-20, Standard Test Methods for Flash Point by Pensky-Martens Closed Cup Tester*, West Conshohocken, PA, 2020.
- 49 P. Ghosh and S. B. Jaffe, *Ind. Eng. Chem. Res.*, 2006, **45**, 346–351.
- 50 A. S. Maheshwari and J. G. Chellani, *Fuel*, 2012, **98**, 55–60.
- 51 A. Vickers, *Higher temperature simulated distillation with DB-HT Sim Dist Columns*, Agilent Technologies, 2002.
- 52 R. M. de Deugd, PhD thesis, Delft University, Netherlands, 2004.
- 53 G. P. van der Laan and A. A. C. M. Beenackers, *Catal. Rev.*, 1999, **41**, 255–318.
- 54 A. De Klerk, *Energy Fuels*, 2009, **23**, 4593–4604.
- 55 Neste Corporation, *Neste Renewable Diesel Handbook*, 2015, pp. 1–33.
- 56 The African Refiners Association (ARA), *ARA policy on African gasoline and diesel specifications*, 2017.
- 57 South African National Standards, SANS 342:2016, 2016, vol. 3.
- 58 J. Requies, J. F. Cambra, M. B. Güemez, U. Izquierdo, P. L. Arias and V. L. Barrio, *Int. J. Hydrogen Energy*, 2012, **38**, 7623–7631.
- 59 J. M. Saad and P. T. Williams, *Fuel Process. Technol.*, 2017, **156**, 331–338.

